Article

Atomistic Simulations of CO and N Diffusion in Silica Zeolites: The Impact of Pore Size and Shape

David Selassie, Disan Davis, Jayme Dahlin, Eric Feise, Greg Haman, David S. Sholl, and Daniela Kohen

More About This Article

Additional resources and features associated with this article are available within the HTML version:

- Supporting Information
- Access to high resolution figures
- Links to articles and content related to this article
- Copyright permission to reproduce figures and/or text from this article

View the Full Text HTML

Atomistic Simulations of CO₂ and N₂ Diffusion in Silica Zeolites: The Impact of Pore Size and Shape

David Selassie,[†] Disan Davis,[†] Jayme Dahlin,[†] Eric Feise,[†] Greg Haman,[†] David S. Sholl,[‡] and Daniela Kohen*,[†]

Chemistry Department, Carleton College, Northfield, Minnesota 55057 and School of Chemical and Biomolecular Engineering, Georgia Institute of Technology, Atlanta, Georgia 30332

Diffusion of CO₂ and N₂, both as single components and as binary mixtures, in three zeolites with identical chemical composition but differing pore structures—silicalite, ITQ-3, and ITQ-7—was studied using atomistic simulations. In all materials CO₂ diffuses slower than N₂, but otherwise the behavior of these gases within ITQ-7 and silicalite is quite different than within ITQ-3. In ITQ-7 and silicalite, the loading dependence of diffusion is very similar for CO₂ and N₂; the apparent activation energies for diffusion of each adsorbate are similar in the two materials, and the diffusion properties of adsorbed mixtures can easily be understood. In contrast, none of these are true within ITQ-3. Free energy and potential energy profiles are used to uncover the roots of these differences. The preferential sites of adsorption for CO₂ and N₂ are the same within ITQ-7 and silicalite but not within ITQ-3. In ITQ-3, CO₂ molecules preferentially adsorb in the windows that separate the material's cages, whereas for N₂ this is the site of the largest barrier to diffusion. As a consequence, CO₂ hinders N₂ diffusion very effectively. Our analysis suggests that this behavior might be common for adsorbates that interact strongly with a material that has narrow windows between cages.

1. Introduction

The diffusion of molecules inside the nanometer-scale pores of zeolites controls the performance of zeolites in many applications of these materials for chemical separations and catalysis.[1,2] For small molecules such as CO₂, understanding the variations in diffusive properties between adsorbed species in different zeolite frameworks may prove critical to selecting appropriate materials for specific applications. Molecular simulations have played a useful role in approaching this issue because with these methods it is possible to probe the properties of diffusing molecules on the atomic length-scales that define the differences between zeolites.[3–6] Simulation methods are now well-developed to examine both self-diffusion and the diffusion coefficients that are relevant to net mass transfer.[7]

A particularly important use of molecular simulations is to examine the properties of adsorbed mixtures.[7–9] Performing and interpreting experiments to characterize mixture diffusion in zeolites in a detailed way is challenging. In molecular simulation, by contrast, treating mixture diffusion is only slightly more involved than treating species adsorbed as single components, at least for mixtures with two or three components. Simulations of mixture diffusion have been used to develop successful correlations for predicting mixture properties from single component data for both self-diffusion[10] and macroscopic diffusion.[11] These correlations can be useful in efforts to screen new nanoporous materials for applications where diffusion is important.[12]

In this paper, we use molecular simulations to examine the diffusion of CO₂ and N₂ in three pure-silica zeolites: silicalite, ITQ-3, and ITQ-7. We have previously described the adsorption properties of CO₂ and N₂ in these three materials,[13] and the

diffusion of a variety of spherical adsorbates in these materials has been described by Skoulidas and Sholl.[14] We report below on both the self- and corrected diffusion coefficients of single component CO₂ and N₂ in each material, as well as the self-diffusion properties of adsorbed mixtures.

Before presenting our results, it is useful to heuristically consider what diffusion properties might be expected in CO₂ and N₂ in silica zeolites. Heuristic expectations can be useful for classifying groups of materials according to their suitability for practical applications. The best example of this type of result is the work by Freeman establishing a fundamental basis for the long-observed tradeoff between selectivity and throughput in polymeric membranes for gas separations.[15] Given the large quadrupole of CO₂, it is not surprising that CO₂ adsorbs considerably more strongly than N₂ in silica zeolites, although the adsorption selectivity does vary among different pore structures.[13] The kinetic diameters of CO₂ and N₂ are quite similar, 0.33 and 0.36 nm,[16] respectively, and are smaller than the narrowest portion of the pores in each material we consider. This observation suggests that neither molecule will face severe steric constraints during diffusion. It is therefore reasonable to expect that the more strongly adsorbing and heavier CO₂ is likely to diffuse slower than N₂. If this expectation is correct, it has important implications for comparing various strategies for using zeolites to separate CO₂ from CO₂/N₂ mixtures. In particular, it implies that membrane-based approaches, where selectivity is determined by a combination of adsorption selectivity and differences in diffusion coefficients, will have less-pronounced selectivities for CO₂ than approaches based purely on adsorption.

It is only a mild extrapolation of the heuristic ideas above to predict that the loading dependence of CO₂ and N₂ diffusion in each material will be similar. That is, it is reasonable to expect that ratio of diffusion coefficients for the two species at low loadings and high loadings are similar. Our results show that this expectation is correct for silicalite and ITQ-7. For ITQ-3,

---

* Corresponding author. E-mail: dkohen@carleton.edu.
† Carleton College.
‡ Georgia Institute of Technology.
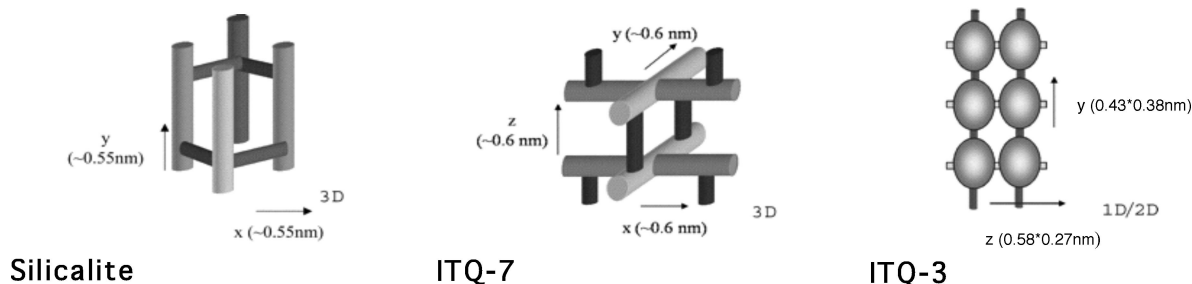
Figure 1. Schematic illustration of pore topology of silicalite, ITQ-7, and ITQ-3. The pore diameters listed for each channel direction give the approximate diameter of the narrowest portion of the pore. This figure was adapted from ref 14.

an interesting and potentially useful deviation from this prediction occurs; at high pore adsorbate densities the single component diffusion coefficients for N_2 are approximately constant whereas for CO_2 they decrease strongly with increasing loading. This difference means that at the highest pore loadings we examined the CO_2 diffusion coefficients are approximately 2 orders of magnitude smaller than those for N_2. We show that this unusual behavior can be understood in terms of the atomic-scale structure of the pores of ITQ-3, and this outcome suggests that a variety of other materials with this interesting property may exist.

The remainder of the paper is structured as follows. In Section 2 we describe our computational methods. Section 3 details our calculated self-diffusion and corrected diffusion coefficients as a function of adsorbate loading for each material. We also present self-diffusion coefficients for a variety of adsorbed mixtures in each material. We show that previously developed correlations based on single component information can accurately predict mixture diffusion coefficients in silicalite and ITQ-7 but that the same approach gives poor results for ITQ-3. In Section 4 we examine the causes of the unusual properties of CO_2 and N_2 in ITQ-3 by comparing them with analogous properties in silicalite and ITQ-7. We conclude in Section 5.

2. Methods and Models

2.1. Atomistic Models for CO_2 and N_2 in Silica Zeolites. As was mentioned in the introduction, the work presented here complements an earlier study of adsorption of CO_2 and N_2 in silica zeolites.[13] Therefore, the atomistic models used here are the same as in that previous work and are only summarized below. Three siliceous zeolites—silicalite, ITQ-3, and ITQ-7—have been chosen to facilitate comparison between several zeolites with differing pore geometries but with identical chemical composition. Figure 1 shows a schematic illustration of pore topology of silicalite, ITQ-7 and ITQ-3.[14] Silicalite (structure type MFI), the all-silica isomorph of ZSM-5, has been extensively studied both experimentally[17–23] and with molecular simulations.[5,24–31] The structure of silicalite's pores is well-known; it has two sets of interconnected 10-ring pores about 5.5 Å in diameter. The straight and sinusoidal channels intersect at right angles, with the channel intersections being slightly larger than the channels themselves.[32] ITQ-3[33] and ITQ-7[34] are two newer siliceous materials. ITQ-7 (structure type ISV) has a three-dimensional system of large pores defined by windows containing 12 member rings of about 6 Å in diameter. ITQ-3 (structure type ITE), on the other hand, has a one-dimensional pore system with small windows of about 4 Å in diameter made up of 8 member rings that open to larger cavities. A second straight channel runs through the material but is too narrow to accommodate guest molecules.

We modeled interactions between adsorbed molecules and the zeolite framework atoms following the method of Mak-

rodimitris et al.[35] That is, each O atom in the zeolite is assumed to interact with each site on the adsorbed molecules through both a Lennard–Jones potential and electrostatic interactions, whereas only electrostatic interactions are considered between adsorbates and Si atoms in the zeolite. We have used the parameters reported by Makrodimitris et al.[35] as model LJCB-.JBTLC because this model is successful in reproducing experimental isotherms for CO_2 and N_2 on silicalite. An important assumption in our work is that potential parameters can be directly transferred to model the same molecules adsorbed in ITQ-3 and ITQ-7. This approach seems plausible because each material has precisely the same composition, but given the absence of experimental data in these two materials, we are unable to directly assess the validity of this assumption. As in most previous atomistic studies of adsorption in zeolites, we assume the adsorbent can be treated as a rigid framework with atomic positions fixed by the observed crystallographic data.[36]
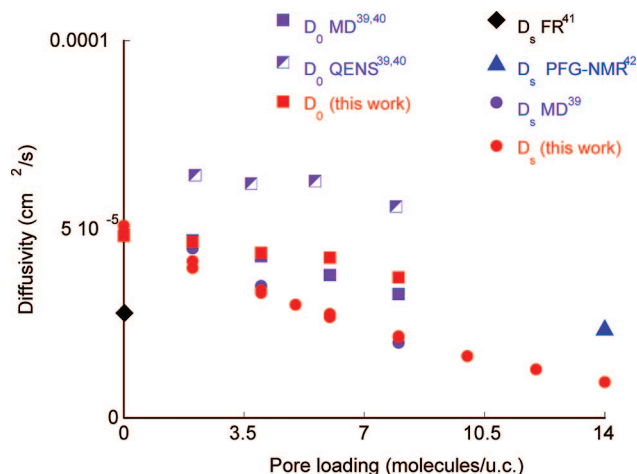
Carbon dioxide was modeled as a linear triatomic and nitrogen as a diatomic molecule with fixed bond lengths and bond angles. Both species were modeled by charged Lennard–Jones (LJ) centers using the TraPPE force field developed by Potoff and Siepmann.[37] These potentials quantitatively reproduce the vapor–liquid equilibria of the neat systems and their mixtures. LJ parameters for the unlike-pairs interactions are calculated with the Lorentz–Berthelot combining rules.[38] Host/guest and guest/guest interactions were modeled by the sum of short-range interaction terms using Lennard–Jones potentials and Coulombic terms accounting for the long-range interaction between the quadrupole moment of the guests and the zeolite's electrostatic field. Periodic boundaries, the minimum image convention, and a 13 Å cutoff were used to properly deal with the short-range interactions. To treat the long-range interactions a 25 Å cutoff was used. In all simulations the simulation box was chosen as containing the smallest number of zeolite unit cells such that its shorter side was longer than twice the largest cutoff.

2.2. Simulation Methods. Molecular dynamics (MD) simulations were performed using methods that are very similar to those described by Skoulidas and Sholl.[24,25] Self-diffusivities (D_s^i) and corrected diffusivities (D_o^i) for each adsorbed component i were calculated from trajectories obtained using equilibrium MD and the corresponding Einstein relationships;

$$D_s^i = \lim_{t \to \infty} \frac{1}{6t} \left\langle \frac{1}{N_i} \sum_{l=1}^{N_i} [r_{l,i}(t) - r_{l,i}(0)]^2 \right\rangle \quad (1)$$

$$D_o^i = \lim_{t \to \infty} \frac{1}{6t} \left\langle \frac{1}{N_i} \left[\sum_{l=1}^{N_i} r_{l,i}(t) - r_{l,i}(0) \right]^2 \right\rangle \quad (2)$$

where N is the number of molecules of species i in the simulation, t is time, $r_{l,i}(t)$ is the position of molecule l of species i at time t, and $\langle \ \rangle$ denotes an ensemble average. Diffusion

CO$_2$ and N$_2$ Diffusion in Silica Zeolites

J. Phys. Chem. C, Vol. 112, No. 42, 2008 **16523**

Figure 2. CO$_2$ single component diffusion coefficients on silicalite at 300 K as computed from MD and observed experimentally.

coefficients in each of the *x*, *y*, and *z* directions were obtained by generalizing the equations above.[24,25] The Einstein definition of the self-diffusion is also valid in binary (or multicomponent) mixtures, and we used this definition to determine self-diffusion in CO$_2$/N$_2$ mixtures. Each MD simulation started with a GCMC pre-equilibration (100 000 Monte Carlo moves) followed by MD equilibration (50 000 MD steps). After equilibration, production runs of 10^6 MD steps were performed using a Nose−Hoover thermostat to keep the temperature constant. The time step in all simulations was 1 fs.

Computing corrected diffusion coefficients requires averaging over multiple calculations; therefore, at least 10 independent runs were performed for each of the results shown. In addition, to ensure equilibration and convergence in our EMD simulations, the number of runs was increased in those calculations with a small number of molecules per unit cell. In all cases reported here, the observed mean square displacements were linear in time, thus the systems were experiencing normal diffusion.

Although loading-dependent transport diffusion coefficients are not below, because they do not offer significant information in the context of this paper, they can be calculated by computing[24,25] $D_t = D_o[(\partial \ln f)/(\partial \ln c)]_T$ where T is temperature and f is fugacity of the bulk phase that is at equilibrium with the adsorbed phase when the loading of the latter is c. The term in parentheses is easily evaluated once adsorption isotherms are known. The adsorption isotherms for each adsorbed component at room temperature has been described in our earlier work.[13]

2.3. Validation of the Models and Simulation Methods. Diffusion of pure N$_2$ and pure CO$_2$ in silicalite has been previously studied experimentally with quasi-elastic neutron scattering,[39,40] frequency response methods,[41] pulsed field gradient-NMR,[42] and molecular simulations.[35,39,40,43] We have used this information to validate our choices of models and simulation methods. Figure 2 shows our MD results for single component diffusion of CO$_2$ at 300 K on silicalite, as well as results from others.[39,41,42] Results for N$_2$ at 200 K show similar trends (results not shown). Very good agreement with previous simulations is obtained for both species. Note that the simulation results of Jobic et al.[39,40] for these systems are in reasonably good agreement with these authors' experimental results. The used parameters appear to provide a reasonable means of describing N$_2$ and CO$_2$ diffusion in silicalite over a broad range of loading, and we conclude that this agreement is good enough to warrant the use of the potentials and methods described earlier.
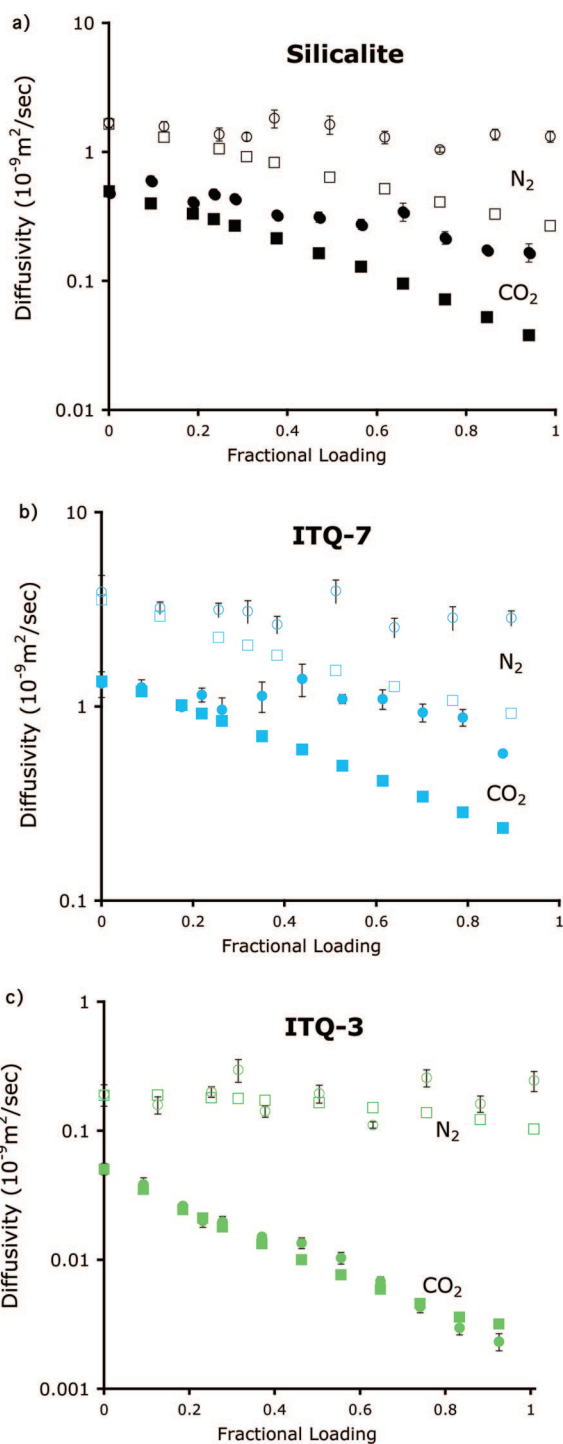
Figure 3. Diffusion coefficients computed from our single-component EMD calculations for CO$_2$ (filled symbols) and N$_2$ (unfilled symbols) in silicalite (a), ITQ-7 (b), and ITQ-3 (c) at 298 K. Squares correspond to Self-diffusion coefficients and circles correspond to Corrected diffusion coefficients.

3. Results and Discussion

3.1. Single Component Diffusion. The diffusion coefficients computed from our single-component EMD calculations for CO$_2$ and N$_2$ in silicalite, ITQ-3, and ITQ-7 at 298 K are shown in Figure 3. Each set of diffusion coefficients is shown as a function of the fractional loading (θ) of the adsorbed species calculated using the saturation loading values derived from the Langmuir fits to the single component adsorption isotherms reported in Goj. et al.[13] Figure 3 shows that diffusion in all materials is fast enough to not hinder most practical applications, although

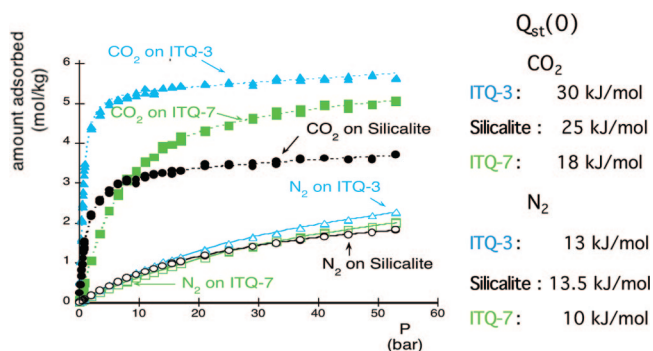**TABLE 1: Self Diffusion Coefficients at Infinite Dilution**

	$D_s^{N_2}(0)$ (10^{-9} m²/sec)	$D_s^{CO_2}(0)$ (10^{-9} m²/sec)
ITQ-7	3.54	1.34
silicalite	1.64	0.49
ITQ-3	0.19	0.05

TABLE 2: Apparent Activation Energy at Infinite Dilution

	$E_a^{N_2}$ (kJ/mol)	$E_a^{CO_2}$ (kJ/mol)
ITQ-7	2.6	4.7
Silicalite	3.1	5.1
ITQ-3	1.1	9.8
	$E_a^{N_2}$ (K)	$E_a^{CO_2}$ (K)
ITQ-7	314	562
Silicalite	375	617
ITQ-3	138	1174

the diffusion coefficients span almost 2 orders of magnitude from the slowest species (CO_2 in ITQ-3) to the fastest (N_2 in ITQ-7). The diffusion coefficients at infinite dilution for both species in each material are listed in Table 1. The infinite dilution value of $D_s^{CO_2}$ in ITQ-3 is 27 times smaller than in ITQ-7, whereas $D_s^{N_2}(0)$ in ITQ-3 is 18 times smaller that in ITQ-7. The infinite dilution diffusion values shown in Figure 3 correlate loosely with heats of desorption (see Figure 4); as expected, the more strongly adsorbed molecules diffuse slower. In all three materials, as was already described for silicalite in the existing literature,[35,39–43] N_2 diffusion is faster than CO_2 diffusion; in all three materials $D_s^{N_2}(0)/D_s^{CO_2}(0)$ is about 3.

The apparent activation energies of self-diffusion were calculated by computing $D_s(0)$ at 200, 298, and 400 K (and 350 K for N_2 within ITQ-3) and then fitting these results to the usual Arrhenius equation. The resulting activation energies are listed in Table 2. In both silicalite and ITQ-7, the apparent activation energy for CO_2 diffusion is ~5 kJ/mol, whereas for N_2 it is ~3 kJ/mol. $D_s(0)$ in these cases correlates loosely with the apparent activation energies. In ITQ-3, the outcome is quite different. In this case, the apparent activation energy for CO_2 is ~10 kJ/mol, whereas for N_2 it is ~1 kJ/mol. This is the first indication in our results that the behavior of N_2 and CO_2 in ITQ-3 are quite different from the other two materials. We examine the roots of this behavior in Section 4.

The variation in the self-diffusion coefficients for each species with loading is summarized in Figure 5, which shows self-diffusion coefficients normalized by their infinite dilution value. In all three materials, the self-diffusion coefficients of both CO_2 and N_2 diminish monotonically with loading. This contrasts with the non-monotonic behaviors that have been seen for some spherical adsorbates in ITQ-3[14] and for some metal−organic framework materials with similar pore topologies.[44] In ITQ-7 and silicalite, the two materials with intersecting channels, $D_s^{N_2}(\theta)/D_s^{N_2}(0)$ and $D_s^{CO_2}(\theta)/D_s^{CO_2}(0)$, decay at a very similar rate. In ITQ-3, the material with cages, the situation is somehow different: $D_s^{CO_2}(\theta)/D_s^{CO_2}(0)$ decays much faster than $D_s^{N_2}(\theta)/D_s^{N_2}(0)$, and both decays are quite different from those seen in silicalite and ITQ-7.

In silicalite and ITQ-7, the corrected diffusivities of CO_2 and N_2 vary only weakly with adsorbate loading. Differences

between the self- and corrected diffusion coefficients at any particular loading are the result of correlations in the motion of individual molecules.[10,11] For silicalite and ITQ-7, the existence of correlations plays an important role in the corrected diffusivity, but our results suggest that the strength of these correlations is similar for each example. As with the self-diffusion coefficient, the behavior of the corrected diffusion coefficients in ITQ-3 is quite different from the other two materials. In ITQ-3, the loading dependence of the corrected diffusivity of both CO_2 and N_2 is very close to the self-diffusion coefficients, especially for CO_2 for which they are essentially identical. We return to this observation later in the context of mixture diffusion.

3.2. Mixture Diffusion. Self-diffusion coefficients computed from our two-component EMD calculations for CO_2 and N_2 mixtures in silicalite, ITQ-3, and ITQ-7 at 298 K are shown in Figure 6. The values are shown as a function of loading in molecules per unit cell (muc). In all materials, N_2 diffuses faster than CO_2 at every loading we examined, as might be anticipated from the relative magnitude of the single component self-diffusion coefficients. The results in Figure 6 shown that in each case, the self-diffusivity of each species decreases as the total pore loading is increased.

In an earlier section we have seen how $D_s^{N_2}$ depends on N_2 loading and how and $D_s^{CO_2}$ depends on CO_2 loading (see Figure 5). The mixtures simulations allow us to study how $D_s^{N_2}$ depends on CO_2 loading and vice-versa. The dependence of $D_s^{CO_2}$ on N_2 loading can be inferred by the slopes marked with an asterisk (*), and the dependence of $D_s^{N_2}$ on CO_2 loading by the slopes marked with a pound sign (#) in Figure 6. It is clear from the figures that CO_2 hinders N_2 diffusion the most in all materials, but the details of the behavior are better seen in Figure 7.

Figure 7 shows the dependence of normalized diffusion coefficients of CO_2 and N_2 for both pure component and equimolar mixtures as a function of total loading. In every case

Figure 4. Isosteric heats (Q_{st}) at infinite dilution and single component adsorption isotherms for CO_2 (filled symbols) and N_2 (unfilled symbols) at 308 K in silicalite (circles), ITQ-3 (triangles), and ITQ-7 (squares) as computed from GCMC and reported by Goj et al.[13]
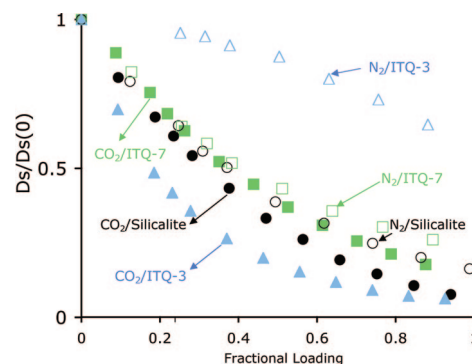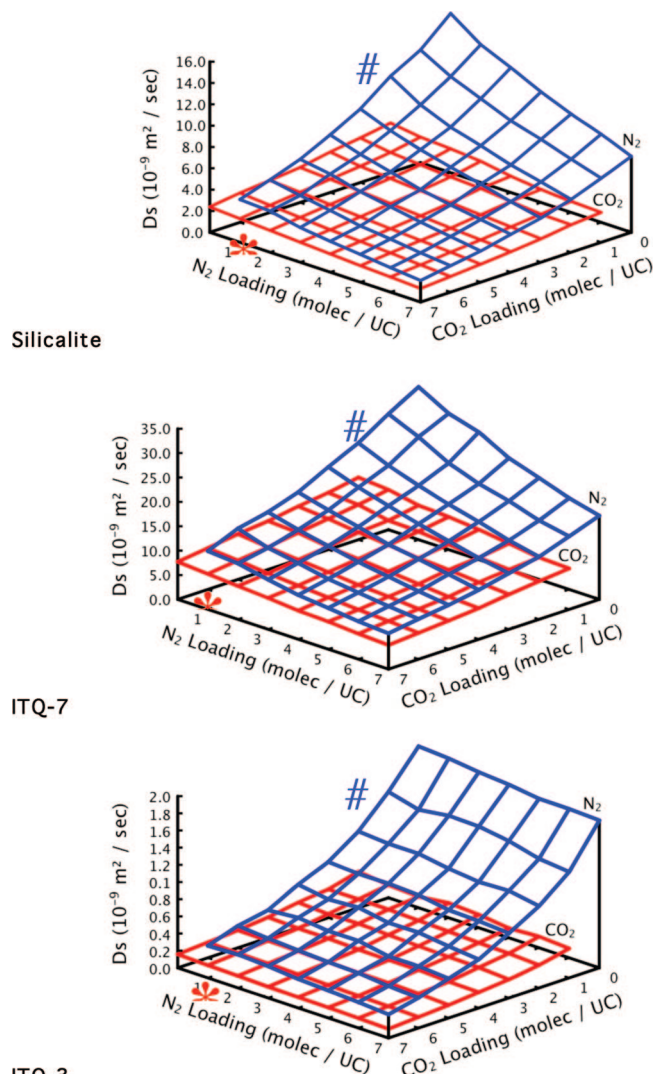

Figure 5. CO_2 and N_2 Self-diffusion coefficients normalized by the corresponding infinite dilution value as a function of fractional loading (θ). Results are presented for CO_2 (filled symbols) and N_2 (unfilled symbols) on silicalite (black circles), ITQ-3 (blue triangles), and ITQ-7 (green squares).
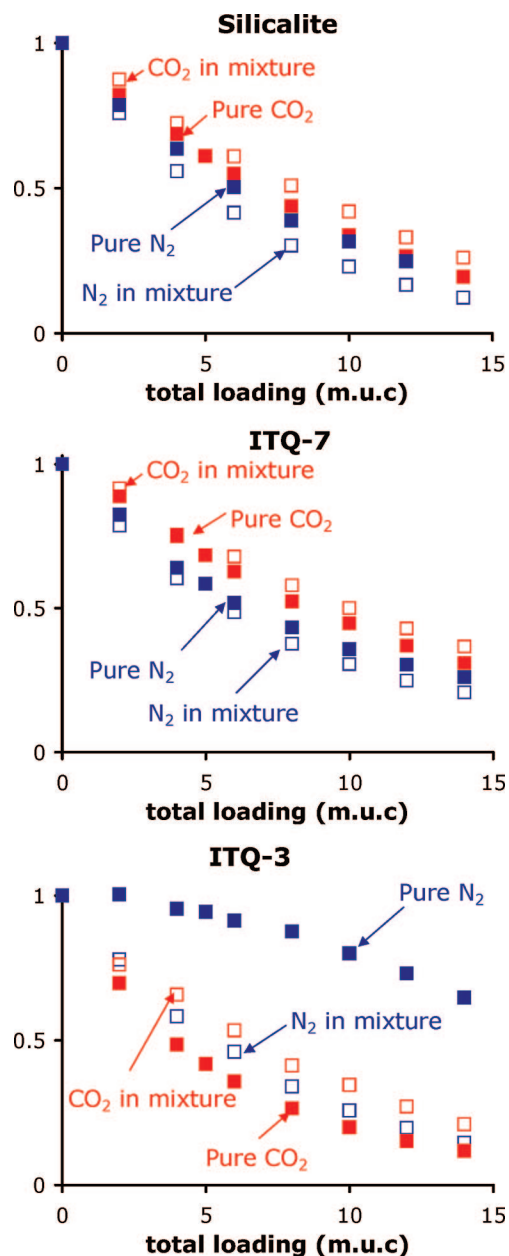
Figure 6. Self-diffusion coefficients computed from our two-component EMD calculations for CO$_2$ and N$_2$ mixtures at 298 K. N$_2$ values are shown in blue and CO$_2$ in red.

shown in this figure, D_s has been normalized to the corresponding values for pure component at infinite dilution. A difference in behaviors of CO$_2$ and N$_2$, within silicalite and ITQ-7 on the one hand and within ITQ-3 on the other, is evident in this figure. Within ITQ-7 and silicalite, the self-diffusion of the more mobile N$_2$ species is slightly lower in the mixture than for the pure species, whereas the self-diffusion of the slower CO$_2$ species is practically the same in the mixture as that in the pure species (when compared at the same total loading). The fact that self-diffusion of CO$_2$ is practically the same for the pure species and the mixture (at the same total loading) suggests that in ITQ-7 and silicalite the identity of the crowding molecules is not very important. The situation is quite different in ITQ-3, where N$_2$ diffuses much more slowly in the mixture than as a pure species, whereas CO$_2$ diffuses virtually as fast in the mixture and as a pure species (again, making comparisons at the same total loading). That is, in ITQ-3, CO$_2$ molecules hinder diffusion more than N$_2$ molecules. The behavior of CO$_2$ molecules hindering the diffusion of other diffusing gases has also been recently observed by Krishna and co-workers[45] when studying the behavior of CO$_2$ and other gases within DDR, another zeolite with narrow pores within cages. These co-workers had attributed this behavior to segregated absorption; later in this paper it will be shown that the same is true in ITQ-3.

3.3. Predicting Binary Self-diffusion Coefficients from Single Component Data. One useful way to analyze results for mixture diffusion is to ask whether the results for adsorbed mixtures can be predicted using only single component information. Krishna and Paschek[10] developed the following correlation to predict mixture self-diffusivities from single component information.

$$D_s^i = \frac{1}{\frac{1}{D_o^i} + \frac{\theta_i}{D_{corr}^{ii}} + \frac{\theta_j}{D_{corr}^{ij}}} \qquad D_s^j = \frac{1}{\frac{1}{D_o^j} + \frac{\theta_j}{D_{corr}^{jj}} + \frac{\theta_i}{D_{corr}^{ji}}} \qquad (3)$$

In this expression, D_s^i is the self-diffusivity of species i in a binary mixture with species j, D_o^i is the pure component corrected diffusivity, D_{corr}^{ii} and D_{corr}^{ij} are the self-exchange and

Figure 7. Normalized self-diffusion coefficients of CO$_2$ and N$_2$ computed from our EMD calculations for both pure component and equimolar mixtures in (a) silicalite, (b) ITQ-7, and (c) ITQ-3 at 298 K vs total loading. N$_2$ diffusion constants are shown in blue and those of CO$_2$ in red. Filled symbols indicate pure component calculations, and unfilled symbols denote equimolar mixtures.

binary-exchange diffusivities that reflect the correlation effects in a mixture,[11] and θ_i is the fractional loading of species i. The corrected diffusivities in this expression are evaluated at the total fractional loading, not at the pure component fractional loading. The self-exchange diffusivities (D_{corr}^{ii}) are defined from single-component data using eq 4.

$$D_s^i(\theta) = \frac{1}{\dfrac{1}{D_o^i(\theta)} + \dfrac{\theta_i}{D_{corr}^{ii}(\theta)}} \qquad (4)$$

The binary-exchange coefficients (D_{corr}^{ij}) must be estimated, and this is done using eq 5,[46]

$$\Theta_{sat}^j D_{corr}^{ij}(\theta) = [\Theta_{sat}^j D_{corr}^{ii}(\theta)]^{\theta_i/(\theta_i+\theta_j)}[\Theta_{sat}^i D_{corr}^{jj}(\theta)]^{\theta_j/(\theta_i+\theta_j)} \qquad (5)$$

where $\Theta_{sat}^j = \theta_j/\theta_{sat}^j$. This correlation has been shown to give accurate results for mixture diffusion in silicalite, carbon nanotubes, and metal—organic framework materials.[11,47,48]

Figures 8 and 9 show the comparison between the self-diffusion results from the binary MD calculations and those predicted using Krishna and Paschek's correlation. Paralleling
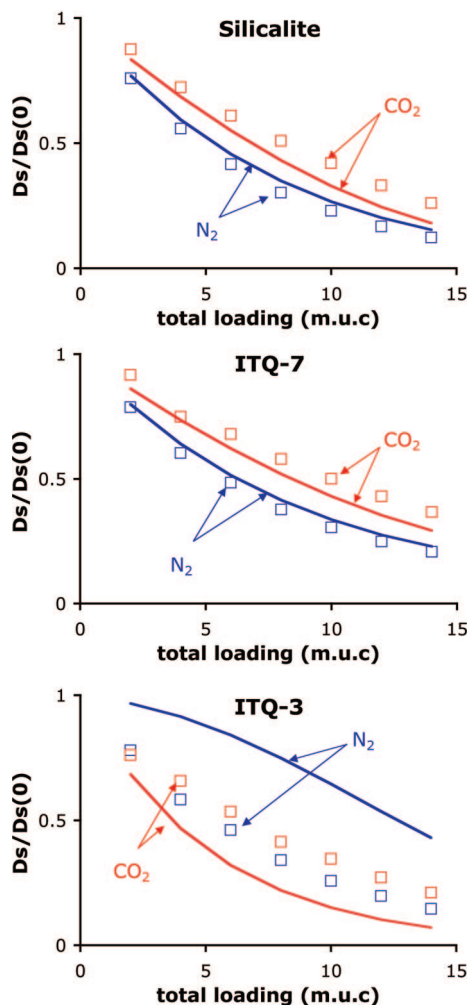
Figure 8. Comparison between the self-diffusion results from the binary MD calculations and those predicted using Krishna and Paschek's formulation. Normalized D_s values are presented as a function of total loading for equimolar mixtures. N_2 diffusion constants are shown in blue, and those of CO_2 are in red. Lines indicate predictions using Krishna and Paschek's formulation, and unfilled symbols denote MD results.
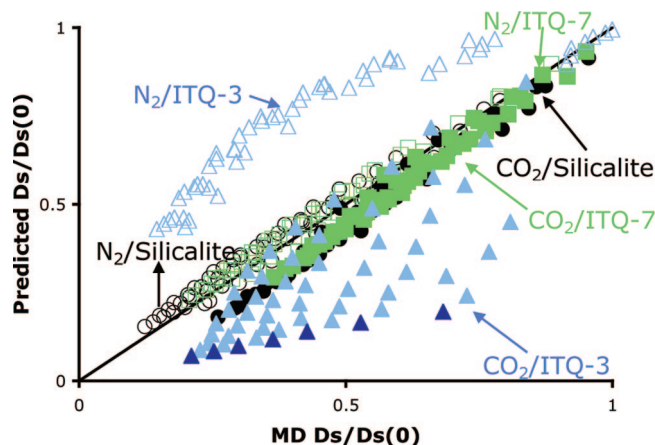
Figure 9. Parity plot between normalized self-diffusion results from the binary MD calculations and those predicted using Krishna and Paschek's formulation. Results are presented for CO_2 (filled symbols) and N_2 (unfilled symbols) on silicalite (black circles), ITQ-3 (blue triangles), and ITQ-7 (green squares). The dark blue triangles correspond to CO_2/ITQ-3 data when the concentration of N_2 is the largest.

Figure 7, in Figure 8 normalized D_s values are presented as a function of total loading for equimolar mixtures. Figure 9 presents a scatter plot of the predictions from the correlation for all loadings/compositions for N_2 and CO_2 in the three materials versus the results obtained in the MD simulations. Note that in order to use eq 5 we have fitted the single component results shown in Figure 3 to functions that achieve an adequate fit; those fits are presented in the Supporting Information.

It is apparent in Figures 8 and 9 that Krishna and Paschek's formulation predicts the behavior of the mixture relatively accurately in ITQ-7 and silicalite, but not so in ITQ-3. The failure is most dramatic within ITQ-3, where the formulation underpredicts the effect of increasing the total loading on $D_s^{N_2}$ at all loadings and overpredicts the effect of increasing the total loading on $D_s^{CO_2}$. The overprediction of the CO_2 diffusivity is especially marked when the concentration of N_2 is the largest (see dark blue data points in Figure 9).

The results of the single component MD simulations showed that within ITQ-3 $D_s^{CO_2}(\theta)$ and $D_o^{CO_2}(\theta)$ were remarkably close (see Figure 3). Earlier it was noted how this indicated that the correlations effects among CO_2 molecules were minimal. In the context of Krishna and Paschek's prediction for mixture self-diffusivities (see eqs 3—5), this results in a very large pure component CO_2 self-exchange coefficient (D_{CO_2}, CO_2), and as a consequence D_{CO_2}, N_2 is very large as well. A very large D_{CO_2}, N_2 value implies vanishing correlations between CO_2 and N_2 molecules, which, as it has been pointed out several times already, is not at all the behavior exhibited by these adsorbates within ITQ-3, so it not surprising that the formulation is not as accurate in this material as it is in ITQ-7, silicalite, and many others.[11,47,48] Equation 4 indicates that the very large value of D_{CO_2}, CO_2 results on $D_s^{CO_2}$ values that depend on total loading but not on the composition of the mixtures, which explains the reasonably good agreement seen in Figure 8c, where $D_s^{CO_2}$ is plotted against total loading for an equimolar mixture, and the worse agreement seen in Figure 9 when the concentration of N_2 is the greatest. It also results in $D_s^{N_2}$ values that depend on total loading but not explicitly on CO_2 loading, which explains the fact that Krishna and Paschek's formulation underpredicts the effect of increasing the CO_2 loading on $D_s^{N_2}$, as shown in Figure 8c.

CO$_2$ and N$_2$ Diffusion in Silica Zeolites

*J. Phys. Chem. C, Vol. 112, No. 42, 2008* **16527**

An underlying assumption of Krishna and Paschek's formulation is that the sites occupied by the adsorbates in the mixture are equivalent. Moreover, the formulation is not designed to take into account situations in which molecules of one species hinder diffusion of molecules of the other species in an asymmetric way. That CO$_2$ and N$_2$ within ITQ-3 do not occupy the same sites, and moreover that there is segregated adsorption occurring within this material, will become clear in the next section.

4. Molecular Understanding of Diffusion in Silicalite, ITQ-7, and ITQ-3

The results detailed above present the following contrasting behaviors within ITQ-3 versus silicalite and ITQ-7: (a) the apparent activation energy of single-component CO$_2$ and N$_2$ self-diffusion in ITQ-3 is very different from the other two materials; (b) the loading dependence of self-diffusion of pure CO$_2$ and N$_2$ differ significantly from one another in ITQ-3, whereas they are similar to each other in the other materials; (c) in ITQ-3 the presence of CO$_2$ in a mixture slows diffusion of both CO$_2$ and N$_2$ much more than the presence of N$_2$; and (d) a correlation that works well for predicting mixture self-diffusion in silicalite and ITQ-7 performs poorly for ITQ-3. In this section these results will be discussed in the context of preferred sites for each species and the free energy and potential energy profiles for diffusion that these molecules experience within each material.

Figure 10 shows probability maps for CO$_2$ (left) and N$_2$ (right) within each material at 298 K and infinite dilution. These maps are normalized 3D histograms of the locations of molecules' center of mass collected during EMD simulations. Equivalent results are obtained if data is collected in a GCMC simulation. For each material, the N$_2$ and CO$_2$ probability maps have the same color scale. In all three materials, the preferred sites are located close to walls rather than in the middle of the channels or intersections. The preferred sites are clearly similar for CO$_2$ and N$_2$ within silicalite and ITQ-7, but this is not the case for ITQ-3. In ITQ-3, CO$_2$ has two distinct types of high probability sites, one inside the material's cages and the other inside the narrow neck connecting adjacent cages. The existence of this second site is somewhat counterintuitive; most previous models of zeolites with similar structures typically envision the neck between cages as a transition state for diffusion of spherical particles.[49] The existence of a similar site has been reported recently, however, for CO$_2$ in DDR, another zeolite with narrow windows connecting larger cages.[45] N$_2$ also shows some tendency to localize in the neck connecting cages in ITQ-3, but in contrast to CO$_2$, the sites that exist within the cages are preferred by N$_2$. This situation also resembles that found by Fritzsche and co-workers[50] when studying diffusion of methane in LTA (another zeolite that has cages connected by windows that resemble short connector channels); these authors found that the preferred locations of CH$_4$ molecules were either in the window or in front of the window, depending on the parameters used to describe the interactions. Because the biggest difference between N$_2$ and CO$_2$ is the strength of their interactions with the zeolite, our results are consistent with this previous work.

A more quantitative way to examine the probability maps introduced above is to integrate these probabilities in a series of planes perpendicular to a reaction coordinate representative of diffusion in each material. We performed integrations of this type for the sinusoidal (*x*-direction) and straight (*y*-direction) channels in silicalite, the two equivalent straight channels in
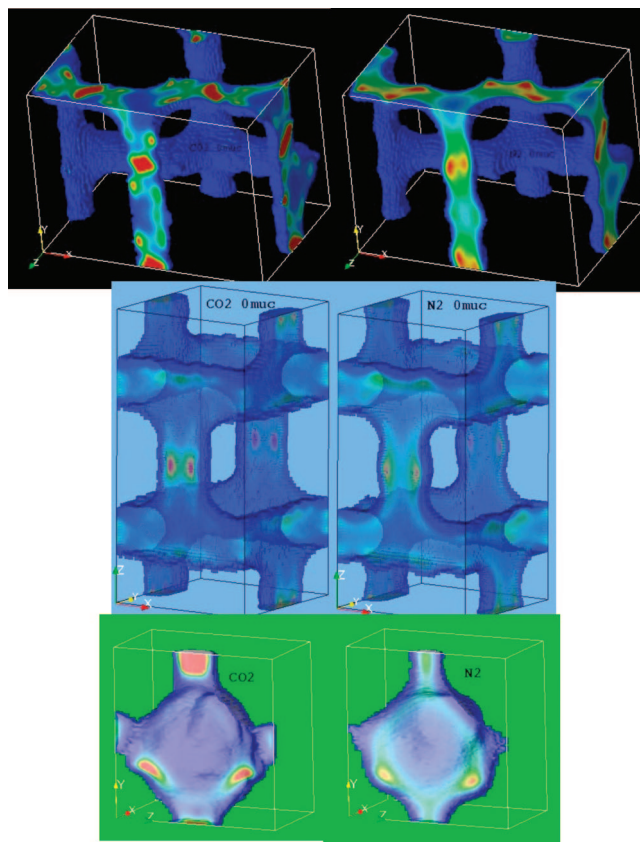

Figure 10. Probability maps for CO$_2$ (left) and N$_2$ (right) at 298 K and infinite dilution in silicalite (black background), ITQ-7 (blue background), and ITQ-3 (green background). For the sake of comparison, for each material the plots have the same color scale. In silicalite a portion of the unit cell is shown, which was chosen to reveal the density in the middle of the straight channel (on the sides) and on the middle of the sinusoidal channel (on the top). For ITQ-7 a unit cell is shown; each picture reveals the density in the middle of both *x* and *y* straight channels and on the middle of the short *z*-channel. (see Figure 1 for a schematic depiction of an unit cell). For ITQ-3 a quarter of the unit cell is shown; each picture displays one cage and reveals the density in the middle of the windows connecting the cages.

ITQ-7, and in ITQ-3 along the *y*-direction. The probability within each relevant channel and its corresponding intersections are isolated during integrations; therefore, the normalized probabilities shown in what follows exclude densities in perpendicular channels. The details of the limits of the integration can be found in the Supporting Information.

Figure 11 compares the integrated probabilities in ITQ-3 with results for the straight channel of silicalite. The outcomes for the sinusoidal channel in silicalite and for ITQ-7 are qualitatively similar to those for the straight channel in silicalite. In silicalite, the overall features of the integrated probability are similar for CO$_2$ and N$_2$, and it is clear that these two species compete for adsorption sites that are similar in character. The situation for ITQ-3, however, is very different. The most notable feature is the lack of N$_2$ probability at the preferred site of CO$_2$, located within the short channel connecting the ITQ-3 cages. Note that although the N$_2$ 3D map in Figure 10 shows some probability in the short connector channels, the probability occupies such a small region of space that the 1D plot shows very little probability in that region. Also note that only one of the two sites that are preferred locations for both CO$_2$ and N$_2$—the one at around 3 Å in Figure 11—was visible in the 3D plots shown earlier; the other could be seen if the pore was cut in the perpendicular direction. Figure 11 reveals the reason underlying
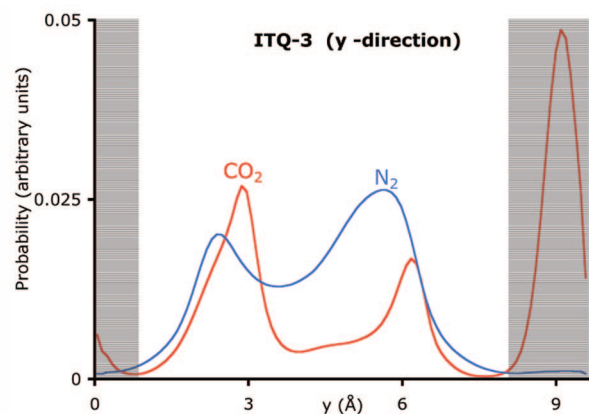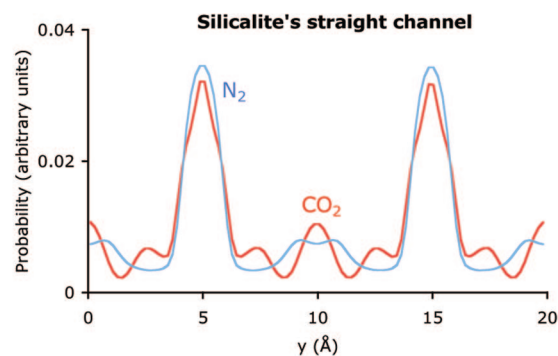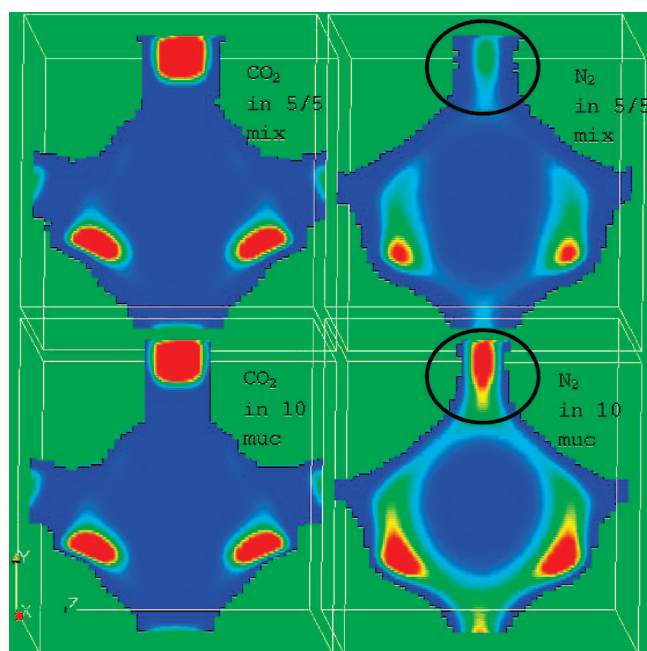
Figure 11. CO_2 center of mass (in red) and N_2 center of mass (in blue) probability along relevant coordinates at 298 K at infinite dilution.

Figure 12. Three-dimensional probability maps for CO_2 (left) and N_2 (right) within ITQ-3 at 298 K. On the top, the maps corresponds to equimolar mixtures of CO_2 and N_2 totaling 10 muc. On the bottom, the CO_2 map corresponds to pure CO_2 at a loading of 10 muc, whereas the N_2 map corresponds to pure N_2 at a loading of 10 muc. For the sake of comparison, all plots have the same color scale.

the poor performance of the correlation approach examined above for predicting mixture self-diffusion. This correlation is based on an assumption that both adsorbing species compete for similar sites in the adsorbent and that mixing on these sites occurs in a simple way. For N_2/CO_2 mixtures in ITQ-3 this idea is clearly not correct because the two species prefer quite different adsorption sites.

Examining the distribution of molecules within the pores of ITQ-3 also reveals why CO_2 molecules hinder the motion of N_2 molecules: by sitting in the narrow passage between cages, CO_2 blocks the motion of other molecules. This idea is strongly support by the probability maps in Figure 12, which show results for CO_2 and N_2 in ITQ-3 adsorbed as equimolar mixtures and as single components. On the top, the maps correspond to an equimolar mixture of CO_2 and N_2, whereas the bottom panels correspond to pure CO_2 and N_2 at the same total loading. The relevant fact is how much less N_2 population resides in the short

channel connecting the cages (this region is emphasized by the circle) when there is CO_2 present than when N_2 is pure. Clearly, the presence of CO_2 hinders the ability of N_2 to cross this crucial region and thus to diffuse from cage to cage.

The behavior within ITQ-3 can be further understood in terms of barriers to diffusion. Figure 13 shows free energy profiles for pure CO_2 and N_2 at two different pore loadings along the relevant diffusion coordinate for ITQ-3 and for the straight channel of silicalite as an example of all other channels studied (data for the other channels is given in the Supporting Information). Free energy profiles are calculated as[51] $\beta F(q) = -\ln \langle P(q) \rangle$ where $P(q)$ are the probabilities shown in Figure 11. First note how the size of the barriers differs among materials. This information is also displayed in Table 3, where ΔF have been calculated as $F_{max}(q) - F_{min}(q)$. The large free energy barrier for diffusion of CO_2 in ITQ-3 points to a possible reason for the similarity between $D_s(\theta)$ and $D_o(\theta)$ for this example. When the barriers to diffusion are large, the motion of multiple CO_2 molecules are likely to be only weakly correlated, so the amount of collective motion that these systems can exhibit is very limited.

For ITQ-3 at infinite dilution the largest barrier for CO_2 diffusion is around 7.5 Å, and a second slightly shallower barrier is around 1 Å in the coordinate shown in Figure 13. These barriers are not in the channels connecting cages, instead they lie at the entrance to this channel. For N_2 in ITQ-3, the largest free energy barrier lies inside the connecting channel. Within silicalite and ITQ-7 the barriers are in the expected locations, which for materials with intersecting channels is in the channels themselves near the intersections.

The nature of the free energy barriers to diffusion can be further understood by examining the relative contribution of energetic and entropic effects. The energetic contribution can be isolated calculating $\langle U(q) \rangle = \int_{x,y \subset \text{channel}} U(x, y, q) e^{-U(x,y,q)/kT}$, where U is the Boltzmann averaged potential energy of 250 molecules that have centers of mass at x, y, q but have random orientations. The entropic contribution can be inferred by using $F = U - TS$. Figure 14 shows $F(q)$ (at infinite dilution) and $U(q)$ at 298 K within ITQ-3 and the straight channel of silicalite (as before, the Supporting Information contains equivalent figures for other channels). Notice that, in general, $U^{N_2}(q)$ is less negative than $U^{CO_2}(q)$, which can be explained by the relatively strong interactions between the quadrupole of CO_2 and the zeolite. The most notable feature these plots reveal is the fact that, within ITQ-3, N_2 has a potential energy minima at the same location as its free energy maxima (the window

CO$_2$ and N$_2$ Diffusion in Silica Zeolites

J. Phys. Chem. C, Vol. 112, No. 42, 2008 **16529**
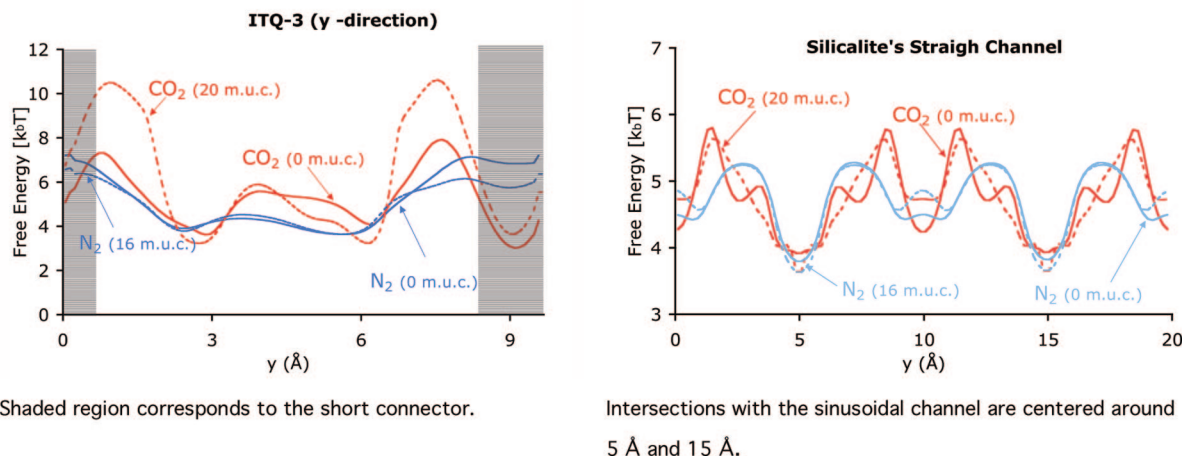
Figure 13. Free energy profiles $F(q)$ for CO$_2$ center of mass (in red) and N$_2$ center of mass (in blue) along relevant coordinates at 298 K. Solid lines correspond to infinite dilution whereas dashed lines correspond to saturation.

TABLE 3

|	ΔF (infinite dilution) (K)	ΔF (saturation) − ΔF (infinite dilution) (K)
ITQ-3 N$_2$	**1075**	**−185**
ITQ-7 N$_2$	**559**	**−50**
ITQ-7 CO$_2$	**535**	**25**
Silicalite Straight CO$_2$	791	31
Silicalite Straight N$_2$	693	39
Silicalite N$_2$ (average)	**644**	**65**
Silicalite Sinusoidal N$_2$	595	91
Silicalite CO$_2$ (average)	**718**	**139**
Silicalite Sinusoidal CO$_2$	644	248
ITQ-3 CO$_2$	**1458**	**745**

between cages). This situation does not occur for CO$_2$ within ITQ-3. This means that the free energy barrier to N$_2$ diffusion is purely entropic in nature. The existence of entropic barriers to diffusion has been described previously for the diffusion of methane in LTA−zeolite.[52,53]

The fact that for CO$_2$ in ITQ-3 the barrier is not located in the narrow connector channel but rather in the entrances to cages is a situation that has not been examined previously by Smit and co-workers[54,55] while using free energy profiles to understand diffusion in nanoporous materials. Although at infinite dilution the behavior of N$_2$ within ITQ-3 can be classified[54] neatly as the behavior within a cage-type zeolite with free energy barriers located in between cages, this is clearly not the case for CO$_2$ within ITQ-3. The fact that similar adsorption sites for CO$_2$ to those we see in ITQ-3 have been reported for adsorption in DDR[45] suggests that there are a number of zeolite structures for which the properties we have seen here may be relevant.

The fact that the location of the preferred adsorption sites and barriers to diffusion exposed by $U(q)$ are different to those exposed by $F(q)$ for N$_2$ within ITQ-3 explains the unusually low value for the apparent activation energy for diffusion discussed in Section 3.1. The Arrhenius description that was used to determine this activation energy captures the energetic contribution to the barrier but not the pre-exponential factor, which takes into account entropic effects. It is not surprising then that when a barrier is entropic in nature, as for N$_2$ in ITQ-3, the low apparent activation energy value superficially fails to account for the fact that N$_2$ diffusion within that material is fairly slow. For CO$_2$ in ITQ-3, the apparent activation energy was the largest of all cases studied, which corresponds nicely

to the slowest diffusion it exhibits and with the fact that the free energy barriers in this case are dominated by the potential energy.

We turn our attention now to the fact that the loading dependence of the self-diffusion coefficients (see Figure 5) is similar for N$_2$ and CO$_2$ within ITQ-7 and silicalite but not within ITQ-3. Figure 13 points to a reason for the difference in behavior as it shows that within ITQ-3 as loading increases the barriers for N$_2$ diffusion diminishes slightly in contrast to the barriers to CO$_2$ diffusion that increase substantially. The fact that the barriers for N$_2$ diffusion diminish as loading increases agrees with both D_s and D_o decreasing very slightly with loading (see Figure 3). Within transition state theory, diffusion rates are proportional to the probability of a molecule being on top of the barrier to diffusion multiplied by a dynamical factor that accounts for events that start at the top of the barrier but do not result in a barrier crossing.[49,56−59] Free energy barriers determine the probability factor and can depend on loading in a nonmonotonic fashion, as seen here, whereas the dynamic factor always monotonically decreases with loading as the probability of random collisions between molecules increases. In this context, we might infer that the fact that as loading increases $D_s^{N_2}$ and $D_o^{N_2}$ diminish slightly within ITQ-3 is simply a result of increasing N$_2$−N$_2$ collisions, because crowding of a narrow passage would have resulted on an entropically driven increase of the free energy in the short connector channel. In contrast, as loading increases the height of the free energy barrier for CO$_2$, diffusion increases dramatically, corresponding with the pronounced loading dependence of CO$_2$ diffusion. Figure 13 also shows how for both CO$_2$ and N$_2$ within the straight channel of silicalite the height of the barriers to diffusion do not change much with loading (the same is true for all other cases, as shown in the Supporting Information), which indicates that the decay of D_o and D_s with loading is most likely caused by the decrease of the dynamical correction factor and not a large decrease of the probability of a molecule being on top of the barrier to diffusion. The relation between the change of the height of the barrier as loading increases and the loading dependence of D_s is further explored in Table 3. It shows how the height of the free energy barrier changes with loading, expressed as ΔF (saturation) − ΔF(infinite dilution). The data is ordered so that the system where the barrier decreases the most with loading (N$_2$ within ITQ-3) is first and the system where the barrier increases the most (CO$_2$ within ITQ-3) is last. This ordering of
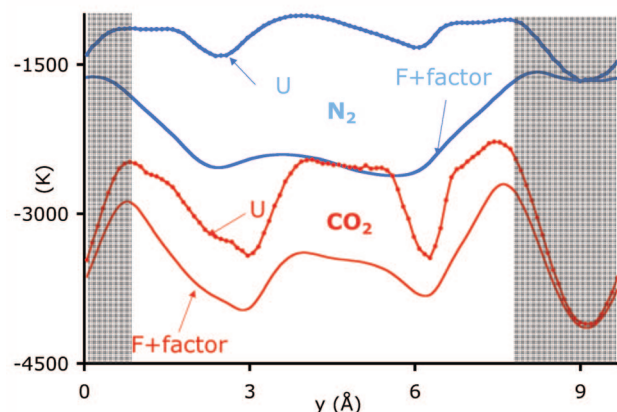
Shaded region corresponds to the short connector.
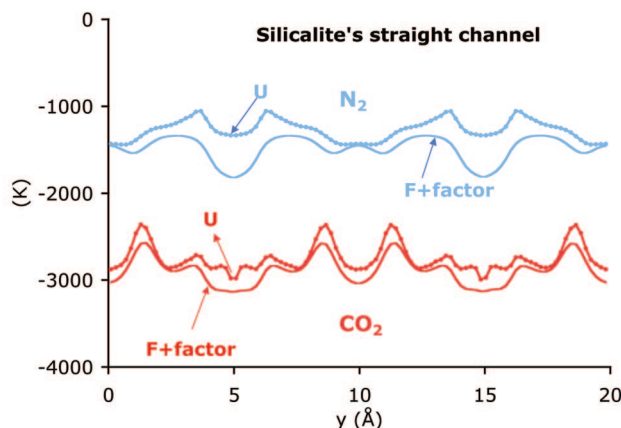
Intersections with the sinusoidal channel are centered around 5 Å and 15 Å.

Figure 14. Free energy profiles ($F(q)$ + factor) and $U(q)$ for CO_2 center of mass (in red) and N_2 center of mass (in blue) along relevant coordinates at 298 K. The factor has been chosen in each case so that the entropy is always arbitrarily positive.

the data in the table reflects the order of the $D_s(\theta)$ curves displayed in Figure 5.

5. Concluding Remarks

We have used molecular simulations to examine the room temperature diffusion of N_2 and CO_2 in three siliceous zeolites, both as pure species and as adsorbed mixtures. In the two channel-type zeolites—silicalite and ITQ-7—the characteristics of the two diffusing species are similar. That is, the loading dependence of the self- and corrected diffusion coefficients are similar for the two species. The main difference between N_2 and CO_2 adsorption in these two materials is that CO_2, which is heavier and has a substantially larger quadrupole moment, diffuses more slowly and has a larger activation energy for diffusion.

The diffusion of N_2 and CO_2 in ITQ-3, a material with cages separated by narrow windows, is different in several interesting ways from the channel-type materials. N_2 diffusion in ITQ-3 is shown to be dominated by the existence of an entropic barrier to diffusion located in the windows between cages. To our knowledge, this is the first study in which free energy profiles are used to characterize an entropic barrier for nonspherical species diffusing in a zeolite. The similarities between N_2 and CO_2 diffusion in other materials might suggest that an entropic barrier may also exist for CO_2 diffusion in ITQ-3. Our

calculations show, however, that the behavior of CO_2 in ITQ-3 is quite different from N_2. Because of its favorable electrostatic interactions with the zeolite framework, CO_2 molecules preferentially bind in the windows between cages in ITQ-3. That is, the sites preferred by N_2 and CO_2 in ITQ-3 are quite different, and the preferred site for CO_2 is the site of the entropic barrier to diffusion of N_2. Because of these differences in location, the loading dependence of the self- and corrected diffusion coefficients for CO_2 and N_2 in ITQ-3 differ markedly from each other.

The differences between N_2 and CO_2 in ITQ-3 have interesting implications for understanding and predicting the diffusion properties of N_2/CO_2 mixtures in this material. For adsorbed mixtures in silicalite and ITQ-7, we found that a correlation developed by Krishna and Paschek accurately predicts the mixture self-diffusion coefficients from single component data. This correlation, however, performs quite poorly for N_2/CO_2 mixtures in ITQ-3. The root of this poor performance is relatively straightforward to understand after characterizing the mechanism for N_2 and CO_2 diffusion as single components in ITQ-3: because these two species do not directly compete for the same adsorption sites, any correlation that implicitly assumes that the adsorbed mixture is a "simple" mixture of the two species will have limited applicability. In this specific case, CO_2 diffusion is only weakly affected by the presence of N_2, since N_2 does not preferentially occupy the favored adsorption sites for CO_2. In contrast, the presence of CO_2 strongly hinders N_2 diffusion because CO_2 molecules preferentially block the sites that act as the free energy barriers for net N_2 diffusion. These results provide an example of how the diffusion properties of simple molecules in zeolites can depend in a sensitive way on the pore structure of the zeolite and suggest that interesting opportunities may exist to achieve interesting separation effects that take advantage of differences in diffusion mechanism between adsorbed molecules in zeolites where diffusion involves molecules moving through narrow pores.

Note Added after ASAP Publication. This paper was published ASAP on September 20, 2008. Figure 7 was updated. The revised paper was reposted on October 16, 2008.

Supporting Information Available: Additional materials mentioned within the text are provided. This material is available free of charge via the Internet at http://pubs.acs.org.

References and Notes

(1) Karger, J.; Ruthven, D. M. *Diffusion in Zeolites and Other Microporous Solids*; John Wiley & Sons: 1992.
(2) Keil, F. J.; Krishna, R.; Coppens, M. O. *Rev. Chem. Eng.* **2000**, *16*, 71.
(3) Heuchel, M.; Snurr, R. Q.; Buss, E. *Langmuir* **1997**, *13*, 6795.
(4) Yang, J. H.; Clark, L. A.; Ray, G. J.; Kim, Y. J.; Du, H.; Snurr, R. Q. *J. Phys. Chem. B* **2001**, *105*, 4698.
(5) Vlugt, T. J. H.; Krishna, R.; Smit, B. *J. Phys. Chem. B* **1999**, *103*, 1102.
(6) Dubbeldam, D.; Calero, S.; Vlugt, T. J. H.; Krishna, R.; Maesen, T. L. M.; Beerdsen, E.; Smit, B. *Phys. Rev. Lett.* **2004**, *93*.
(7) Sholl, D. S. *Acc. Chem. Res.* **2006**, *39*, 403.
(8) Sanborn, M. J.; Snurr, R. Q *Aiche J.* **2001**, *47*, 2032.

CO$_2$ and N$_2$ Diffusion in Silica Zeolites

J. Phys. Chem. C, Vol. 112, No. 42, 2008 **16531**

(9) Sanborn, M. J.; Snurr, R. Q. *Sep. Purif. Technol.* **2000**, *20*, 1.

(10) Krishna, R.; Paschek, D *Phys. Chem. Chem. Phys.* **2002**, *4*, 1891.

(11) Skoulidas, A. I.; Sholl, D. S.; Krishna, R. *Langmuir* **2003**, *19*, 7977.

(12) Keskin, S.; Sholl, D. S. *J. Phys. Chem. C* **2007**, *111*, 14055.

(13) Goj, A.; Sholl, D. S.; Akten, E. D.; Kohen, D. *J. Phys. Chem. B* **2002**, *106*, 8367.

(14) Skoulidas, A. I.; Sholl, D. S. *J. Phys. Chem. A* **2003**, *107*, 10132.

(15) Freeman, B. D. *Macromolecules* **1999**, *32*, 375.

(16) Aguilar-Armenta, G.; Patino-Iglesias, M. E.; Leyva-Ramos, R. *Adsorpt. Sci. Technol.* **2003**, *21*, 81.

(17) Golden, T. C.; Sircar, S. *J. Colloid Interface Sci.* **1994**, *162*, 182.

(18) Sun, M. S.; Shah, D. B.; Xu, H.; Talu, O. *J. Phys. Chem. B* **1998**, *102*, 1466.

(19) Jobic, H.; Skoulidas, A. I.; Sholl, D. S. *J. Phys. Chem. B* **2004**, *108*, 10613.

(20) Skoulidas, A. I.; Bowen, T. C.; Doelling, C. M.; Falconer, J. L.; Noble, R. D.; Sholl, D. S. *J. Membr. Sci.* **2003**, *227*, 123.

(21) Bonilla, G.; Tsapatsis, M.; Vlachos, D. G.; Xomeritakis, G. *J. Membr. Sci.* **2001**, *182*, 103.

(22) Lai, Z. P.; Bonilla, G.; Diaz, I.; Nery, J. G.; Sujaoti, K.; Amat, M. A.; Kokkoli, E.; Terasaki, O.; Thompson, R. W.; Tsapatsis, M.; Vlachos, D. G. *Science* **2003**, *300*, 456.

(23) Nair, S.; Tsapatsis, M. *J. Phys. Chem. B* **2000**, *104*, 8982.

(24) Skoulidas, A. I.; Sholl, D. S. *J. Phys. Chem. B* **2001**, *105*, 3151.

(25) Skoulidas, A. I.; Sholl, D. S. *J. Phys. Chem. B* **2002**, *106*, 5058.

(26) Newsome, D. A.; Sholl, D. S. *J. Phys. Chem. B* **2005**, *109*, 7237.

(27) Krishna, R.; Vlugt, T. J. H.; Smit, B. *Chem. Eng. Sci.* **1999**, *54*, 1751.

(28) Krishna, R.; Paschek, D. *Phys. Chem. Chem. Phys.* **2001**, *3*, 453.

(29) Clark, L. A.; Gupta, A.; Snurr, R. Q. *J. Phys. Chem. B* **1998**, *102*, 6720.

(30) Snurr, R. Q.; Bell, A. T.; Theodorou, D. N. *J. Phys. Chem.* **1994**, *98*, 11948.

(31) Newsome, D. A.; Sholl, D. S. *J. Phys. Chem. B* **2006**, *110*, 22681.

(32) Olson, D. H.; Kokotailo, G. T.; Lawton, S. L.; Meier, W. M. *J. Phys. Chem.* **1981**, *85*, 2238.

(33) Camblor, M. A.; Corma, A.; Lightfoot, P.; Villaescusa, L. A.; Wright, P. A. *Angew. Chem., Int. Ed.* **1997**, *36*, 2959.

(34) Villaescusa, L. A.; Barrett, P. A.; Camblor, M. A *Angew. Chem., Int. Ed.* **1999**, *38*, 1997.

(35) Makrodimitris, K.; Papadopoulos, G. K.; Theodorou, D. N. *J. Phys. Chem. B* **2001**, *105*, 777.

(36) Fuchs, A. H.; Cheetham, A. K. *J. Phys. Chem. B* **2001**, *105*, 7375.

(37) Potoff, J. J.; Siepmann, J. I. *AIChE J.* **2001**, *47*, 1676.

(38) Allen, M. P.; Tildesley, D. J. *Computer Simulations of Liquids*; Oxford Science Publications; Oxford, 1994.

(39) Jobic, H.; Makrodimitris, K.; Papadopoulos, G. K.; Schober, H.; Theodorou, D. N *Stud. Surf. Sci. Catal.* **2004**, *154B*, 2056.

(40) Papadopoulos, G. K.; Jobic, H.; Theodorou, D. N. *J. Phys. Chem. B* **2004**, *108*, 12748.

(41) Shen, D. M.; Rees, L. V. C. *J. Chem. Soc., Faraday Trans.* **1994**, *90*, 3011.

(42) Karger, J.; Pfeifer, H.; Stallmach, F.; Feoktistova, N. N.; Zhdanov, S. P. *Zeolites* **1993**, *13*, 50.

(43) Demontis, P.; Karger, J.; Suffritti, G. B.; Tilocca, A. *Phys. Chem. Chem. Phys.* **2000**, *2*, 1455.

(44) Skoulidas, A. I.; Sholl, D. S. *J. Phys. Chem. B* **2005**, *109*, 15760.

(45) Krishna, R.; van Baten, J. M. *Chem. Phys. Lett.* **2007**, *446*, 344.

(46) Krishna, R.; van Baten, J. M. *J. Phys. Chem. B* **2005**, *109*, 6386.

(47) Krishna, R.; van Baten, J. M *Ind. Eng. Chem. Res.* **2006**, *45*, 2084.

(48) Keskin, S.; Liu, J.; Johnson, J. K.; Sholl, D. S. *Langmuir*. in press.

(49) Tunca, C.; Ford, D. M. *J. Chem. Phys.* **1999**, *111*, 2751.

(50) Fritzsche, S.; Haberlandt, R.; Hofmann, G.; Karger, J.; Heinzinger, K.; Wolfsberg, M. *Chem. Phys. Lett.* **1997**, *265*, 253.

(51) Dubbeldam, D.; Beerdsen, E.; Vlugt, T. J. H.; Smit, B. *J. Chem. Phys.* **2005**, *122*, 224712.

(52) Schuring, A.; Auerbach, S. M.; Fritzsche, S.; Haberlandt, R. *J. Chem. Phys.* **2002**, *116*, 10890.

(53) Beerdsen, E.; Dubbeldam, D.; Smit, B. *J. Phys. Chem. B* **2006**, *110*, 22754.

(54) Beerdsen, E.; Dubbeldam, D.; Smit, B. Phys. Rev. Lett. 2006, *96*.

(55) Beerdsen, E.; Dubbeldam, D.; Smit, B. Phys. Rev. Lett. 2005, *95*.

(56) Eyring, H. *J. Chem. Phys.* **1935**, *3*, 107.

(57) Evans, M. G.; Polanyi, M. *Trans. Faraday Soc.* **1935**, *31*, 0875.

(58) Chandler, D. *J. Chem. Phys.* **1978**, *68*, 2959.

(59) Bennett, C. H. In *Diffusion in Solids: Recent Developments*; Academic Press: New York, 1975; p 77.